Biogeosciences Discuss., 9, 14291–14325, 2012
www.biogeosciences-discuss.net/9/14291/2012/
doi:10.5194/bgd-9-14291-2012

Biogeosciences Discussions

Diapycnal oxygen supply to the tropical North Atlantic oxygen minimum zone

T. Fischer, D. Banyte, P. Brandt, M. Dengler, G. Krahmann, T. Tanhua, and M. Visbeck

Helmholtz Centre for Ocean Research (GEOMAR), Kiel, Germany

Received: 1 October 2012 – Accepted: 2 October 2012 – Published: 17 October 2012

Correspondence to: T. Fischer (tfischer@geomar.de)

Published by Copernicus Publications on behalf of the European Geosciences Union.

Abstract

The replenishment of consumed oxygen in the open ocean oxygen minimum zone (OMZ) off West Africa in the tropical North Atlantic Ocean is studied, with a focus on oxygen transport across density surfaces (diapycnal flux). The latter is obtained from a large observational set of oxygen profiles and diapycnal mixing data from years 2008 to 2010. Diapycnal mixing is inferred from different sources: a large scale tracer release experiment, microstructure profiles, and shipboard acoustic current measurements plus density profiles. The average diapycnal diffusivity in the study area is $1 \times 10^{-5}\,m^2\,s^{-1}$. No significant vertical gradient of average diapycnal diffusivities exists in the depth interval from 150 to 500 m. The diapycnal flux is found to contribute substantially to the oxygen supply of the OMZ. Within the OMZ core, 1.5 $\mu mol\,kg^{-1}\,a^{-1}$ of oxygen is supplied via diapycnal mixing, contributing about a third of the total demand. The oxygen that is contributed via diapycnal mixing originates from oxygen that has been laterally supplied within the overlying Central Water layer by advective and eddy fluxes. Due to the existence of a separate shallow oxygen minimum at about 100 m depth throughout most of the study area, there is no direct net vertical oxygen flux from the surface layer of the study area into the Central Water layer. Thus all oxygen supply of the OMZ is associated with remote pathways.

1 Introduction

The open oceans host distinct permanent regions of low oxygen concentration (oxygen minimum zones OMZs), many of them situated at eastern boundaries in the tropics outside the equatorial belt. Tropical OMZs have common features in their coinciding with weak mean circulation and in their typical core depth range of 200 to 700 m, but their spatial extent and overall oxygen levels are diverse, with relatively high values in the Atlantic compared to the Indian and Pacific Oceans (Karstensen et al., 2008; Paulmier and Ruiz-Pino, 2009). OMZs are regions of diverse microbial and biochemical

BGD
9, 14291–14325, 2012

activity (Lam and Kuypers, 2011; Wright et al., 2012), but pose a challenge or even lethal threat to certain marine animal species, with increasing numbers of threatened species the lower the oxygen level (Vaquer-Sunyer and Duarte, 2008; Ekau et al., 2010; Prince et al., 2010).

Being situated below the euphotic layer, the existence and position of oxygen minimum layers can be explained by a balance between oxygen loss by respiration of organic matter (consumption) and oxygen supply (excess of influx over outflux) that results from ventilation (Wyrtki, 1962). Density coordinates subdivide oxygen flux into isopycnal and diapycnal components, i.e. along and across surfaces of constant density. In steady state there must be a balance between *consumption rate* and *divergence of isopycnal flux* and *divergence of diapycnal flux*. This balance is assumed to hold to first order despite some slow changes discussed below. The consumption rate may be seen as an external forcing exerted by sinking organic matter that originates in the surface layer, while parameters of ocean circulation like mean flow and eddy diffusivities set the system's reaction: the emanating shape of the oxygen concentration field and the size of associated oxygen fluxes. In this view, feedbacks on organic matter supply by long-term changes in circulation parameters are ignored.

For the future in the wake of a warming ocean with increasing stratification, a net decline of the global ocean oxygen content is expected, and with it an expansion and intensification of OMZs is anticipated (Keeling et al., 2010). Consequences of oxygen decline for biogeochemical cycles, marine organisms and ecosystems are expected to be profound, particularly in regions that are already low in oxygen (Ekau et al., 2010; Gruber, 2011; Wright et al., 2012). Observations over the past decades indicate a recent decline in global subsurface ocean oxygen content (Stramma et al., 2010; Helm et al., 2011), with some exceptions particularly in the subtropical gyres (Stramma et al., 2010), as well as a recent expansion of individual OMZs: outside the tropics (Whitney et al., 2007; Bograd et al., 2008) and in the tropical Atlantic and Pacific Oceans (Stramma et al., 2008b). Model simulations do not well reproduce the observed global oxygen distribution (Duteil and Oschlies, 2011; Najjar et al., 2007; Meissner et al.,

BGD
9, 14291–14325, 2012

2005); nonetheless they consistently predict global ocean oxygen loss under future climate scenarios (Keeling et al., 2010). What will happen to extent and intensity of individual OMZs in the future, is however less clear. Oxygen solubility, stratification, circulation, and organic export production are all processes that can be affected by climate change (Bopp et al., 2001, 2002), and each of them, by their effect on ventilation and consumption, sensitively influences the extent and intensity of OMZs (Gruber, 2011). Simulation efforts have resulted in projections of future global OMZ volume from expansion (Matear and Hirst, 2003; Oschlies et al., 2008) to neutral (Gruber, 2011) to contraction (Duteil and Oschlies, 2011). The latter study found all three possible trends, with the sign of the predicted trend being sensitive to the amount of background diapycnal mixing. Supply path research is still rated a critical issue at the base of OMZ process understanding and the ability to predict OMZ fate (Keeling et al., 2010). Despite ongoing progress (e.g. Brandt et al., 2010; Banyte et al., 2012), uncertainties concerning size and relative importance of supply paths and processes remain.

Here we report on observed diapycnal mixing, and the corresponding diapycnal oxygen supply, in the tropical North Atlantic OMZ, i.e. an OMZ that has shown a noticeable oxygen decline during the last 5 decades (Stramma et al., 2008b, 2009). In the framework of the German research programmes SFB754, SOPRAN, and NORTH ATLANTIC and the EU project EUROSITES, observation activities intensified in this region since 2008, with several cruises to the tropical North Atlantic OMZ. A large scale tracer release experiment (GUTRE, Guinea Upwelling Tracer Release Experiment) in the oxycline above the OMZ core provided an integrative view on diapycnal diffusivity (Banyte et al., 2012). An extensive grid of local measurements of diapycnal diffusivity performed by microstructure profiling and shipboard acoustic current profiling, together with oxygen profiles, provided an independent approach and statistical background information. Based on these data sources we constrain diapycnal mixing in the tropical North Atlantic OMZ, from which we are able to estimate the average diapycnal oxygen supply as a function of density. This in turn also provides some constraints to the isopycnal oxygen supply and OMZ supply paths.

BGD
9, 14291–14325, 2012

2 Study site

2.1 Tropical North Atlantic oxygen minimum zone

The OMZ in the tropical North Atlantic Ocean (Fig. 1) approximately matches the Guinea Dome region (Siedler et al., 1992). This coincidence is most likely caused by both, OMZ and Guinea Dome, being linked to the zone of weak circulation between North Equatorial Current (NEC at 20° N to 15° N) and North Equatorial Countercurrent/Undercurrent (NECC/NEUC at 5° N) (Karstensen et al., 2008). Vertical oxygen profiles in this region typically exhibit two oxygen minimum layers at core depths of about 100 m and 450 m (Fig. 4). The shallow minimum exists in about 80 to 90 % of our observations, with observations that lack a shallow minimum being scattered throughout the area, but becoming more frequent towards the southern edge of the OMZ. The oxygen minimum at about 450 m exists in all profiles in the region, and in the following we will only study this deeper, more voluminous and more intense oxygen minimum. Its core is at the interface between Antarctic Intermediate Water (AAIW) and the overlying Central Water (Stramma et al., 2008a). The vertical position of the core in the OMZ region does neither perfectly follow isobaths nor isopycnals (Fig. 2). However it is better aligned to isopycnals: the standard deviation of the core vertical position in the OMZ is 60 m with respect to the mean core depth of 425 m, and 40 m with respect to the mean core isopycnal 27.03 kg m^{-3}. The position of the maximum oxygen gradient above the OMZ core (at about 300 m depth) will be called "deep oxycline" throughout this study, in order to distinguish it from the oxycline just below the mixed layer (Fig. 4). We define horizontal OMZ extent by the 60 µmol kg^{-1} isoline of oxygen core concentration as observed between 2008 and 2010 (Fig. 1). The region encompassed by this isoline excludes better ventilated adjacent regimes, particularly those associated with the eastward flow of the NECC/NEUC in the South and with the subtropical gyre at Cape Verde front in the North. Meridional oxygen variations in the OMZ are found to be associated with a system of alternating zonal current bands, in which eastward currents coincide with higher oxygen concentration (Stramma et al., 2008a; Brandt et al., 2010).

BGD
9, 14291–14325, 2012

2.2 Analysis box

For the analysis of diapycnal oxygen flux, a box is chosen from 6 to 15° N latitude, 30 to 15° W longitude, and 150 to 500 m depth. This analysis box covers large parts of the OMZ at its 60 µmol kg^{-1} isoline of core concentration, and it is centered at the location of the lowest observed core concentrations just below 40 µmol kg^{-1} (Fig. 1). Nevertheless it omits some parts of the OMZ: to the Northeast a region associated with upwelling, to the West a part where we expect core concentrations between 50 and 60 µmol kg^{-1}, and to the Southeast a part inside the shelf region and exclusive economic zones of some West African states. The chosen analysis box is the place where diapycnal mixing can be constrained best, because it was horizontally and vertically filled with tracer in the later phase of tracer release experiment GUTRE (after 20 and 30 months), and because most supplemental diapycnal mixing measurements that are suitable for our analysis were conducted during GUTRE surveys inside the analysis box (Fig. 3). The chosen depth interval extends from below the shallow oxygen minimum via the deep oxycline down to the core of the deep oxygen minimum (Fig. 4). Thus our analysis is confined to the upper half of the deep oxygen minimum layer, and diapycnal oxygen flux to the OMZ from the well oxygenated waters below the OMZ will not be considered in this study. Stratification (N^2) is near constant through the chosen depth interval for individual profiles but varies from 1×10^{-5} to 2×10^{-5} s^{-2} in the region with higher values found towards the Southeast (e.g. Banyte et al., 2012).

3 Data and methods

3.1 Diapycnal diffusivity, diapycnal flux, diapycnal flux divergence and averaging

Diapycnal diffusivity K will be used to describe diapycnal mixing and to estimate the diapycnal flux of watermass properties. Due to the presence of turbulence in the ocean,

BGD
9, 14291–14325, 2012

diapycnal property fluxes are greatly enhanced compared to property fluxes in a non-turbulent fluid. Diapycnal diffusivities are thus strongly governed by the turbulent flow characteristics of the oceanic region, albeit in principle K must be differentiated with respect to the watermass property in focus. As in our case the appropriate K_{oxygen} is inaccessible, approximate estimates had to be used. In this study, three different measurement methods are used to estimate K: from the diapycnal spreading of a tracer during GUTRE (Sect. 3.4), from direct measurements of the strength of turbulence using microstructure shear profiles (Sect. 3.5) and from vessel mounted Acoustic Doppler Current Profiler (vmADCP) data (Sect. 3.6). While GUTRE delivered an estimate of K_{tracer} (or K_{TRE}), with the tracer supposedly behaving similar to dissolved oxygen, microstructure and vmADCP measurements delivered an estimate of K_ρ, the diapycnal diffusivity of mass.

The diapycnal oxygen flux Φ can be estimated using Fick's first law of diffusion if simultaneous profiles of oxygen concentration (Sect. 3.3) and diapycnal diffusivity are available. The diapycnal flux is a down gradient flux perpendicular to density surfaces, driven by diapycnal diffusivity. The necessary diapycnal gradient of oxygen concentration to calculate Φ can be approximated by the vertical gradient of oxygen concentration, so that

$$\Phi = -\rho\, K_c\, \frac{\partial}{\partial z} c \tag{1}$$

with ρ water density in $\mathrm{kg\,m^{-3}}$, K_c diapycnal diffusivity of oxygen in $\mathrm{m^2\,s^{-1}}$, c oxygen concentration in $\mu\mathrm{mol\,kg^{-1}}$ and resulting diapycnal flux Φ in $\mu\mathrm{mol\,m^{-2}\,s^{-1}}$.

When regarding the oxygen budget in a volume enclosed by two isopycnal surfaces, the diapycnal influx across the first isopycnal surface does not need to be of the same magnitude as the diapycnal outflux across the second isopycnal surface. The difference of the two diapycnal fluxes is described by diapycnal flux divergence $\nabla\Phi$, which can be approximated by the vertical derivative of Φ, $\partial\Phi/\partial z$. $\nabla\Phi$ is in $\mu\mathrm{mol\,kg^{-1}\,a^{-1}}$. A positive value means that the density layer loses oxygen via a diapycnal flux imbalance. In order

BGD
9, 14291–14325, 2012

to quantify net oxygen supply of the density layer caused by diapycnal processes, it is necessary to observe $-\nabla\Phi$.

Ultimately, the goal is to determine averaged profiles of diapycnal diffusivities, fluxes and flux divergences for the entire OMZ. Thus averaging along isopycnal surfaces is a necessary processing step which will be denoted by brackets, e.g. as in $\langle K \rangle$. Unless otherwise specified the brackets mean arithmetic averaging after objective mapping on isopycnal surfaces. For the objective mapping, the decorrelation scale was determined to 0.5°. Additionally, averaging in diapycnal direction will occur and will be denoted by an overbar, e.g. as in $\overline{K}$, so that a total average for the entire analysis box in this example would be $\langle \overline{K} \rangle$.

3.2 Data overview

The data was collected during 4 cruises in November 2008 (R.V. Merian MSM10/1), November and December 2009 (R.V. Meteor M80/1 and M80/2) and October 2010 (R.V. Meteor M83/1), during the tracer surveys for GUTRE. Oxygen was measured using a Conductivity-Temperature-Depth profiler (CTD) with added Clark-type oxygen sensors (CTD-O_2). For most of the oxygen profiles, simultaneous estimates of diapycnal diffusivity K_ρ from microstructure profiles or vmADCP were available. In total, 400 complete profiles consisting of CTD-O_2 and diapycnal diffusivity were collected in the analysis box (Fig. 3). The tracer surveys delivered one additional independent space-time-averaged estimate of diapycnal diffusivity for the entire region for 2008 through 2010. Another 3 cruises in February, March, and April 2008 (R.V. L'Atalante GEOMAR/3 and GEOMAR/4, and R.V. Merian MSM08/1) delivered 110 additional oxygen profiles without simultaneous K estimates. These oxygen measurements helped in outlining the OMZ (Fig. 1), but did not enter the oxygen flux calculation.

BGD
9, 14291–14325, 2012

3.3 Oxygen and CTD data calibration

Each ship station that is considered here comprises a CTD-O_2 profile, down to at least the deep oxygen minimum core at about 400 to 500 m. On the four cruises evaluated here (MSM10/1, M80/1, M80/2, and M83/1) similar CTD/rosette systems were used, consisting of a Seabird 911plus CTD equipped with dual Seabird temperature, conductivity, and oxygen sensors. During each of the cruises several hundred water samples were collected to calibrate the conductivity and oxygen sensors using a Guildline Autosal 8400B salinometer and a Winkler titration stand. The deviations between the in situ conductivity measured by the Seabird CTD and the high accuracy on-board water sample measurements using salinometers were used to derive a correction to the CTD's conductivity linear in pressure, temperature, and CTD conductivity itself. After applying the corrections, the resulting absolute accuracy of the CTD salinity values was estimated to 0.005, 0.002, 0.002, and 0.003 for the cruises MSM10/1, M80/1, M80/2, and M83/1, respectively. Laboratory calibration suggests the accuracy of the temperature and pressure measurements to be better than 0.002 K and 1.5 dbar, respectively. Similar to conductivity, the deviations between the CTD and the on-board Winkler titrations were used to derive a correction to the CTD's oxygen measurements. The chosen correction was linear in pressure, temperature, and oxygen, and we estimate the absolute accuracy of the CTD's oxygen measurements to be better than 3, 1, 1, and 1 $\mu mol\,kg^{-1}$ for the four cruises, respectively.

While these estimates of the CTD data's absolute uncertainty and their only slowly varying corrections are useful for comparisons with other observations, for our analysis of vertical oxygen gradients an estimate of the oxygen sensor noise and precision is more relevant. We found that the oxygen sensors had a typical instrument noise of less than 0.2 $\mu mol\,kg^{-1}$. The estimates of vertical oxygen gradients used here are based on 1 dbar averages of the CTD oxygen measurements, which were originally recorded at 24 Hz. This results in a noise-induced uncertainty of the vertical oxygen gradient of less than 0.03 $\mu mol\,kg^{-1}\,m^{-1}$ when evaluated at 2 dbar intervals.

BGD
9, 14291–14325, 2012

3.4 K estimated from GUTRE

The deliberate Guinea Upwelling Tracer Release Experiment (GUTRE) was performed in the deep oxycline in the tropical North Atlantic OMZ, in order to obtain a time- and space-integrated estimate of diapycnal diffusivity at the OMZ's upper limit. 92 kg of the halocarbonic compound SF_5CF_3 (Ho et al., 2008) were released in April 2008 at 8° N 23° W at the isopycnal surface σ_θ = 26.88 kg m^{-3}. The expanding tracer patch was sampled during 3 survey campaigns (MSM10/1, M80 and M83/1) 7, 20 and 30 months after injection. After 20 and 30 months, the tracer essentially covered the analysis box horizontally and vertically. From the increase of the vertical extent of the isopycnally integrated tracer distribution, the time-space-averaged diapycnal diffusivity was estimated to be $\langle \overline{K} \rangle_{\mathrm{TRE}} = (1.19 \pm 0.18) \times 10^{-5}\,\mathrm{m^2\,s^{-1}}$ (Banyte et al., 2012). The uncertainty on 95 % confidence level is based on bootstrapping and measurement errors. During all 3 surveys the mean tracer concentration profile showed no significant skew.

3.5 K estimated from microstructure data

As an independent method from GUTRE, diapycnal diffusivities were also estimated using microscale shear recordings from a loosely-tethered microstructure profiler. During the tracer survey cruises, the microstructure profiler MSS90D (termed MSS in the following) of Sea and Sun Technology, Trappenkamp, Germany, was used immediately after certain CTD casts. Usually 3 profiles in a series down to 500 m at 0.5 m s^{-1} sink velocity were collected at these ship stations. In total, MSS data could be obtained on 45 ship stations in the analysis box.

On the way to estimate diapycnal diffusivities from MSS, the signal from 2 to 4 airfoil shear sensors at the profiler head was converted to profiles of microscale vertical shear. Then the dissipation rate ϵ of turbulent kinetic energy could be estimated from the power spectrum of microscale vertical shear, by using a vertical wavenumber range free of instrument vibrational noise and by assuming local isotropy (Oakey, 1982; Stips and Prandke, 2000). The diapycnal diffusivity of mass, K_ρ, was inferred from the

BGD
9, 14291–14325, 2012

Osborn parametrization $K_\rho = \Gamma\, \epsilon\, N^{-2}$ (Osborn, 1980) with Γ the dimensionless dissipation ratio that is related to mixing efficiency. Γ was set 0.2, because simulation data by Shih et al. (2005) suggest this value to be appropriate for weak to moderate turbulence, what is what was found in the analysis box. The value 0.2 is further supported by findings of St. Laurent and Schmitt (1999), who report Γ between 0.15 and 0.25 in turbulence dominated regimes with weak mean shear, conditions that were also met in the analysis box. For the analyses of this study, vertical averages of ϵ and N^2 for the depth interval 150 m through 500 m were used to infer a single average $\overline{K}_{\rho,\mathrm{MSS}}$ per ship station via the Osborn parametrization. The uncertainty of $\overline{K}_{\rho,\mathrm{MSS}}$ was estimated from quantifiable errors (essentially from sensor uncertainties and spectral estimation) to be 60 % on a 95 % confidence level.

3.6 K estimated from vmADCP

The possibility to obtain additional estimates of K_ρ from current velocity profiles via vmADCP substantially enhanced the number of "complete" station data comprising CTD plus oxygen plus K, which could be used to infer diapycnal oxygen flux; the number rising from 45 to 400 inside the analysis box (Fig. 3). The method is based on the observation that finescale vertical shear with vertical wavelengths of order 10 m to some 100 m and dissipation rate ϵ of turbulent kinetic energy can be related (Gargett, 1976; Gregg, 1989). It had been used before with Lowered ADCP data (Polzin et al., 2002; Kunze et al., 2006). The main processing strategy for the application to vmADCP data during ship stations was: (1) generate velocity profiles with noise low enough, so that vertical shear signals can still be detected which are on the order of the open ocean background level; (2) obtain spectra of vertical shear of horizontal velocity, in finescale vertical wavenumber range; (3) obtain dissipation rate ϵ from shear power spectral level Φ_S by a parametrization (see appendix), which uses MSS measurements for calibration; (4) obtain K_ρ from ϵ and CTD derived stratification by the Osborn parametrization as in Sect. 3.5.

BGD
9, 14291–14325, 2012

Minutiae of processing were: During 3 survey cruises MSM10/1, M80/2 and M83/1, an RDI Ocean Surveyor 75 kHz vmADCP continuously recorded currents down to 600 m depth at 8 m vertical bin size. The broadband mode that we used, a high ping frequency (36 min^{-1}), usually calm sea conditions, and a final two-dimensional filtering step of velocity fields in depth-time-space, resulted in one-minute-average velocity data of 1 $cm\,s^{-1}$ precision at 95 % level (for technical details refer to Fischer, 2011). From the one-minute-averaged and filtered velocity profiles, spectra of vertical shear were calculated for 150 to 533 m depth and corrected following Polzin et al. (2002) for variance losses caused by ADCP binning, tilting and ping averaging. The resulting one-minute shear power spectra were usable in the wavenumber band from 1/128 cpm to 1/38.4 cpm. Power spectra were averaged over the duration of a ship station, and served to estimate a single value of shear power spectral level Φ_S for that ship station and the entire depth interval 150 to 500 m. Φ_S led to $\overline{\epsilon}_{ADCP}$ after using the parametrization Eq. (A5), and to $\overline{K}_{\rho,ADCP}$ after using the Osborn parametrization. The uncertainty of $\overline{\epsilon}_{ADCP}$ was estimated to be 60 % on 95 % confidence level, resulting from measurement noise, discrete spectrum estimation, and error progression through the parametrization Eq. (A5).

3.7 Implications of *K* derived from different sources

Apart from physical differences of the derived diapycnal diffusivities, the 3 applied methods delivered K estimates, which also differ in the grade to which they represent spatial and temporal averaged quantities. The immediate result of the MSS measurements were vertical profiles of K_ρ for each ship station at about 0.5 m depth resolution, the result of the vmADCP processing was a single vertical average $\overline{K}_\rho$ for each ship station, and the TRE delivered essentially one time-space-average $\langle\overline{K}\rangle$ for the entire analysis box during 2008 to 2010. For the further processing of K – i.e. to deliver estimates of $\langle\overline{K}\rangle$, a profile of diapycnal oxygen flux, $\langle\Phi\rangle$, and a profile of diapycnal flux divergence – we assume that K can be treated as vertically homogeneous through the used depth

BGD
9, 14291–14325, 2012

interval 150 to 500 m for timescales larger than several days. This assumption gets supported by the MSS derived average K_ρ profile $\langle K_\rho \rangle_{\mathrm{MSS}}$, which shows no significant gradient in 150 to 500 m (Fig. 4), as well as by GUTRE tracer profiles, which showed no significant deviation from a Gaussian (Banyte et al., 2012). Vertical homogeneity in 150 to 500 m is also suggested by the majority of individual density profiles in the analysis box, which show a near constant stratification. The assumption of vertically homogeneous K implies that (1) vertical averaging of K for MSS data is equivalent to averaging of longer timeseries, which we lack; (2) $\overline{K}$ defines the level of the assumed constant K profile at each ship station; in that sense K and $\overline{K}$ are equivalent for the process of isopycnal averaging (e.g. to estimate $\langle \Phi \rangle$).

Another property of our dataset is the statistical independence of K_ρ resp. $\overline{K}_\rho$ from MSS/ADCP and the corresponding oxygen gradient, as shown in Fig. 5 for all depths between 150 and 500 m. The independence is expressed in the equivalence of $\langle K_\rho \times \mathrm{grad}\, c \rangle$ and $\langle K_\rho \rangle \times \langle \mathrm{grad}\, c \rangle$. This also means that $\langle \Phi \rangle$ may be calculated as $\langle \langle K \rangle \times \mathrm{grad}\, c \rangle$, i.e. K may also be treated as if it was laterally homogeneous (but this time on the long timescale of the TRE duration). The estimates of this effective long-term largescale K will be denoted $\langle \overline{K} \rangle_{\mathrm{TRE}}$ and $\langle \overline{K} \rangle_{\mathrm{MSS/ADCP}}$ (MSS and ADCP combined, because the ADCP method was calibrated with MSS measurements).

4 Results and discussion

4.1 Diapycnal diffusivities

Estimates of diapycnal diffusivity were derived from the deliberate tracer release experiment GUTRE and from MSS/ADCP methods. The different estimates are evaluated by comparing the box average $\langle \overline{K} \rangle_{\mathrm{MSS/ADCP}}$, calculated from microstructure measurements enhanced by vessel mounted ADCP, to the GUTRE value $\langle \overline{K} \rangle_{\mathrm{TRE}}$. From MSS/ADCP we find an average diapycnal diffusivity of mass of $\langle \overline{K} \rangle_{\mathrm{MSS/ADCP}}$

BGD
9, 14291–14325, 2012

$= 0.95 \times 10^{-5}\,\mathrm{m^2\,s^{-1}}$ with 95 % confidence interval [0.91 1.08]$\times 10^{-5}\,\mathrm{m^2\,s^{-1}}$ which has been estimated by a bootstrap method. Banyte et al. (2012) report a tracer diapycnal diffusivity of $\langle\overline{K}\rangle_{\mathrm{TRE}} = 1.19\times 10^{-5}\,\mathrm{m^2\,s^{-1}}$ with 95 % confidence interval [1.01 1.37]$\times 10^{-5}\,\mathrm{m^2\,s^{-1}}$ (Sect. 3.4). The difference between $\langle\overline{K}\rangle_{\mathrm{MSS/ADCP}}$ and $\langle\overline{K}\rangle_{\mathrm{TRE}}$ is moderate but significant: the probability to find this or a greater difference is 2 %, when two independent measurement methods are applied to estimate the value of $\langle\overline{K}\rangle$, and these methods have uncertainties according to the two reported confidence intervals.

There are several possible physical reasons for the diffusivity of a passive tracer, K_{TRE}, and the diffusivity of mass, K_ρ, to be different. One fundamental difference between the two is related to double diffusive processes: in salt finger regimes, salt and other passive tracers are transported more effectively than buoyancy; thus tracer diffusivities are enhanced. In our case this would mean to get a low-biased value of $\langle\overline{K}\rangle$ when using $\langle\overline{K}\rangle_{\mathrm{MSS/ADCP}}$ for an estimate. St. Laurent and Schmitt (1999) report for another TRE site in the subtropical North Atlantic (NATRE), that double diffusion can make up for the difference that was found here between K_{TRE} and K_ρ. In order to estimate the relative importance of double diffusion, double diffusive enhancement of K was estimated from CTD profiles following St. Laurent and Schmitt (1999), with salt-finger thermal diffusivity $k_\theta^{(f)}$ assumed to be $6\times 10^{-6}\,\mathrm{m^2\,s^{-1}}$. Applying this method to the depth interval 150 to 500 m suggests that double diffusive enhancement could add $0.1\times 10^{-5}\,\mathrm{m^2\,s^{-1}}$ to $\langle\overline{K}\rangle_{\mathrm{MSS/ADCP}}$ in the upper part of the Central Water, then be negligible for ±50 m above and below the deep oxycline, while sharply rising just at the OMZ core depth to $0.3\times 10^{-5}\,\mathrm{m^2\,s^{-1}}$ and further rising to $0.5\times 10^{-5}\,\mathrm{m^2\,s^{-1}}$ below the core depth. For the entire 150 to 500 m depth interval this would result in an effective enhancement of $\langle\overline{K}\rangle_{\mathrm{MSS/ADCP}}$ by roughly $0.1\times 10^{-5}\,\mathrm{m^2\,s^{-1}}$, which in turn would make the difference between $\langle\overline{K}\rangle_{\mathrm{MSS/ADCP}}$ and $\langle\overline{K}\rangle_{\mathrm{TRE}}$ insignificant.

Besides this possible explanation for the difference between $\langle\overline{K}\rangle_{\mathrm{MSS/ADCP}}$ and $\langle\overline{K}\rangle_{\mathrm{TRE}}$, the two methods to estimate $\langle\overline{K}\rangle$ further contain systematic biases of unknown

BGD
9, 14291–14325, 2012

amount that could not be accounted for in the methods' uncertainties. Concerning the TRE this applies to (1) the fact that for each tracer survey about half of the tracer patch could not be sampled and thus the deduced diapycnal extent of the patch might be biased; (2) $\langle \overline{K} \rangle_{\mathrm{TRE}}$ being biased towards the early TRE period in which the tracer did only cover a fraction of the entire region. Concerning MSS measurements this applies to (1) underlying assumptions in the train of calculating turbulent diffusivity (e.g. the value of dissipation ratio Γ in the Osborn parametrization), (2) seasonal bias, (3) some gaps in the sampling of the analysis box. We interpret the similarity of the two estimated $\langle \overline{K} \rangle$ values as indication that the unaccounted systematic biases are small. But we cannot decide which of the two $\langle \overline{K} \rangle$ estimates is better, and thus leave the two for further calculations, in their difference representing the additional uncertainty in estimated diapycnal diffusivity that results from applying different methods.

The average diapycnal diffusivity that we find for the analysis box is distinctly higher than expected for this latitude range. An internal wave field with background intensity and with stratification in the found range of 1 to 2 $\times 10^{-5}\,\mathrm{s}^{-2}$ should exhibit a $\langle \overline{K} \rangle$ of only some $10^{-6}\,\mathrm{m}^2\,\mathrm{s}^{-1}$ following the parametrization in Gregg et al. (2003). The discrepancy in $\langle \overline{K} \rangle$ is coincident with rough bottom topography in the analysis box and an intensified internal wave field (Fischer, 2011).

4.2 Diapycnal oxygen flux in the analysis box

Diapycnal diffusivities and oxygen gradients are combined to an average profile of diapycnal oxygen flux as function of density for the analysis box (Fig. 6). Here the depth interval 150 to 500 m, for which we know K, roughly corresponds to the potential density range of $\sigma_\theta = 26.55\,\mathrm{kg\,m}^{-3}$ to $27.1\,\mathrm{kg\,m}^{-3}$ in a near linear relation. Main features of the diapycnal oxygen flux profile are two layers of zero flux which correspond to positions of zero oxygen gradient in the mean oxygen profile, and a maximum oxygen downflux at the deep oxycline inbetween. The lower layer of zero diapycnal flux at $\sigma_\theta = 27.03\,\mathrm{kg\,m}^{-3}$ is in the OMZ core depth and means that the OMZ can be separated

BGD
9, 14291–14325, 2012

into an upper and a lower half and that oxygen supply can be assessed separately for these OMZ halves. The depth interval of our data only allows calculations for the upper half of the OMZ. The upper layer of zero diapycnal flux at $\sigma_\theta = 26.63\ \mathrm{kg\,m^{-3}}$ is situated in the overlying Central Water that carries a relatively high oxygen concentration, and it exists because of the widespread presence of a shallow oxygen minimum above. The existence of the layer of zero diapycnal flux means that in the analysis box the oxygen supply to the OMZ has no direct link to the surface ocean. The diapycnal downflux of oxygen at the deep oxycline ($\sigma_\theta = 26.85\ \mathrm{kg\,m^{-3}}$) is about $(5 \pm 1) \times 10^{-3}\ \mu\mathrm{mol\,m^{-2}\,s^{-1}}$. This may be interpreted as a diapycnal supply of about 1.5 $\mu\mathrm{mol\,kg^{-1}\,a^{-1}}$ from the overlying Central Water to the upper half of the OMZ, or as a redistribution of oxygen inside the water body that is limited by the two layers of zero diapycnal flux.

4.3 Sensitivity to data processing

The processing of the diapycnal flux profile was performed in various ways, with respect to the measurement method for K and the sequence order of processing steps, in order to explore the sensitivity of the result to processing decisions. The reference method to obtain diapycnal flux, as defined by us, was calculating local flux profiles from local $K_{\mathrm{MSS/ADCP}}$ and local oxygen gradients in small (2 m) intervals, then averaging local flux profiles isopycnally to an aggregated flux profile and finally smoothing vertically (in a symbolic notation: $\langle K_{\mathrm{MSS/ADCP}} \times \mathrm{grad}\, c \rangle_{\mathrm{smoothed}}$). Other ways of processing were tested against this reference. Swapping isopycnal averaging and flux calculation ($[\langle K_{\mathrm{MSS/ADCP}} \rangle \times \langle \mathrm{grad}\, c \rangle]_{\mathrm{smoothed}}$) has, as expected, little effect since $K_{\mathrm{MSS/ADCP}}$ and $\mathrm{grad}\, c$ are statistically independent in our dataset (Sect. 3.7). Thus using $\langle \overline{K} \rangle_{\mathrm{TRE}}$ to calculate diapycnal flux by $[\langle \overline{K} \rangle_{\mathrm{TRE}} \times \langle \mathrm{grad}\, c \rangle]_{\mathrm{smoothed}}$ essentially differs from $\langle K_{\mathrm{MSS/ADCP}} \times \mathrm{grad}\, c \rangle_{\mathrm{smoothed}}$ by the factor $\langle \overline{K} \rangle_{\mathrm{TRE}}$ / $\langle \overline{K} \rangle_{\mathrm{MSS/ADCP}}$. The attempt to reduce measurement error by smoothing local oxygen gradient profiles before both calculating flux and averaging isopycnally (i.e. $\langle \overline{K} \rangle_{\mathrm{TRE}} \times \langle \mathrm{grad}\, c_{\mathrm{smoothed}} \rangle$ vs.

BGD
9, 14291–14325, 2012

$[\langle\overline{K}\rangle_{TRE} \times \langle \mathrm{grad}\, c\rangle]_{smoothed}$) not only reduces noise but also systematically reduces the gradient and thus the estimated diapycnal flux (Fig. 6).

4.4 Sensitivity to coordinate choice

It may be worthwhile asking what the diapycnal flux across other surfaces than isopycnals is, even though then diapycnal flux is no longer perpendicular to these surfaces and there also exists an isopycnal flux component across these surfaces. Obvious coordinate choices other than isopycnal could be isobaths or surfaces that are linked to features of the oxygen field. Such a different choice primarily changes the vertical shift with which profiles of oxygen gradient get aggregated in the process of averaging laterally (i.e. along the surfaces appropriate for the chosen coordinate system). We examined two cases: (1) diapycnal flux across isobaths, (2) diapycnal flux across a surface that connects the gradient maxima of the deep oxycline. For case (1) the resulting diapycnal flux profile is similar in shape to the diapycnal flux profile of Fig. 6, but flux values are reduced by about 30 %; the downward diapycnal flux at the deep oxycline is about 3×10^{-3} to 4×10^{-3} µmol m^{-2} s^{-1}. A coordinate choice like in case (2) leads to the maximum possible estimate of downward diapycnal flux at the deep oxycline; here the resulting flux is about 6×10^{-3} to 7×10^{-3} µmol m^{-2} s^{-1}.

4.5 Diapycnal flux divergence and OMZ oxygen budget

Looking at the oxygen budget for individual isopycnal layers of the OMZ (Fig. 7) allows further insight into oxygen supply than just quantifying the oxygen flux across particular surfaces. The contribution to oxygen supply by diapycnal processes, i.e. diapycnal surplus in units of moles oxygen per volume and time, is described by a negative diapycnal flux divergence (Sect. 3.1). Maximum diapycnal contribution happens at about the OMZ core, zero diapycnal contribution at the maximum oxygen gradients above and below the OMZ core. The overlying Central Water loses oxygen to the OMZ below by diapycnal mixing, but also upwards towards the shallow oxygen minimum layer. Concerning

BGD
9, 14291–14325, 2012

the other terms of the oxygen budget – consumption rate and isopycnal supply –, consumption rate estimates may be taken from literature, while isopycnal supply is the difference of consumption rate and diapycnal supply, assuming steady state. Reported consumption rate profiles are diverse and uncertain (Keeling et al., 2010), but their principal shape is typically assumed to be exponential with depth (Martin et al., 1987; Karstensen et al., 2008). Karstensen et al. (2008) estimated an exponential consumption rate profile specific for the Atlantic and Pacific OMZ regions from apparent oxygen utilization and estimated water ages. This profile is used here: consumption rate in $\mu mol\,kg^{-1}\,a^{-1}$ is $-0.5 + 12 \cdot \exp(-0.0021 \cdot z)$ with z depth in meters. The uncertainty of the consumption rate was estimated to be 40 % (95 % confidence level) from the scatter of Karstensen et al. (2008)'s reported oxygen utilization rates. Thus the resulting uncertainty of the deduced profile of isopycnal supply is large, but the main pattern seems clear: the profile of isopycnal oxygen supply resembles a step function, with large isopycnal supply in the Central water layer above the deep oxycline, and little isopycnal supply in the OMZ layer below the deep oxycline. The contribution of diapycnal supply to the OMZ core may be estimated to be about a third of the demand, with large uncertainty.

5 Conclusions

The tracer release experiment and the MSS/ADCP measurements complement each other and delivered consistent estimates of diapycnal diffusivity K. For the 400 stations in the analysis box, which covers large parts of the OMZ in the depth interval 150 to 500 m in the thermocline, we found statistical independence of local diapycnal diffusivity and local vertical oxygen gradient. This feature allows to estimate average diapycnal flux in the analysis box from the regional average of diapycnal diffusivity and the regional average of the oxygen gradient profile, given that these averages are representative for the analysis box. If such an independence of K and the concentration

BGD
9, 14291–14325, 2012

gradients is also valid for other regions and substances, regional diapycnal fluxes may be estimated from datasets which comprise non-simultaneous measurements.

The estimated oxygen budget suggests that diapycnal mixing contributes substantially to oxygen supply of the tropical North Atlantic OMZ. In the layers of the analysis box associated with the OMZ core, about a third of total oxygen supply is diapycnal. Such a rating of importance however depends on perspective and the chosen boundaries, and potentially is subject to some adjustments when better estimates of isopycnal supply and consumption rate become available. It might be equally valid to assign the oxygen supply entirely to lateral processes: if choosing a layer bounded by isopycnal surfaces σ_θ = 26.63 kg m^{-3} and 27.03 kg m^{-3} (each with zero diapycnal flux), the supply of the water column inbetween must be completely isopycnal and the role of diapycnal mixing would reduce to just generating internal oxygen redistribution. But even with this latter perspective, the role of diapycnal mixing is substantial. If diapycnal mixing was less intense than observed, the oxygen distribution in the analysis box would certainly be another: given the other parameters kept constant, the vertical oxygen gradient would most likely become sharper and the oxygen concentration in the OMZ core would become lower. In sum we conclude that the higher than expected level of diapycnal mixing in the study region (Sect. 4.1) plays a substantial role in shaping the oxygen concentration field and supposedly also in causing relatively high levels of oxygen in the core of the tropical North Atlantic OMZ compared to other OMZs.

The importance of diapycnal flux to supply the lower half of the deep OMZ with oxygen from AAIW can only hardly be evaluated with the present data, which mostly did not reach the necessary depths. But there are indications that the diapycnal influence is substantial as well. Although gradient and curvature of oxygen concentration are known to be lower in the lower half than in the upper half of the OMZ, turbulent diffusivity below the OMZ core is found equal or larger than above (Fig. 4), and is enhanced by double diffusion here (adds 50 % if following the method of St. Laurent and Schmitt, 1999). The resulting total diapycnal oxygen flux from below might even reach similar values as from above, while the oxygen consumption rate to be balanced is lower than

BGD
9, 14291–14325, 2012

above. A scheduled TRE starting by the end of 2012 aims at estimating isopycnal and diapycnal diffusivity around the OMZ core and will elucidate the relative importance of supply processes; together with ADCP and microstructure profiles down to 1000 m.

Local profiles of consumption rate are still difficult to obtain (e.g. Keeling et al., 2010), but are important for closing the budget. Nevertheless, the general tendency of consumption rate to diminish with depth seems described well enough by the fitted exponential of Karstensen et al. (2008), and moderate deviations from that profile would not change the main features of the deduced isopycnal oxygen supply profile as of (Fig. 7). In fact, some deviation from an exponential shape seems even probable, e.g. caused by active organic matter transport during diel vertical migration of zooplankton (Angel, 1985; Steinberg et al., 2002). The local importance of the latter process for the OMZ region is unknown, but acoustic evidence of strong migrant activity suggests enhanced oxygen consumption at about 300 m and diminished oxygen consumption at about 200 m depth. This is a shape not uncommon in reported consumption profiles (Feely et al., 2004 for the Pacific), but on their reported level the effect would just be shifting the jump in the isopycnal supply profile of Fig. 7 slightly downwards, while not changing the profile's principal shape.

Concerning the shape of the deduced isopycnal supply profile, the sharp decline at the depth of the deep oxycline (Fig. 7) could principally originate from diffusive and/or advective supply. However we do not expect lateral diffusivities having a jump at the deep oxycline, nor expect a vertical jump of proper sign in the second derivative of isopycnal oxygen distribution (supported by WOA09 climatological data; Garcia et al., 2010). This makes eddy processes an improbable reason for the sharp decline. Further we do not expect mean current velocities having a jump in magnitude or direction at the depth of the deep oxycline. Thus it is suggested that the main contribution to the shape of isopycnal oxygen supply is due to mean advection of water with oxygen profiles of greater than average vertical oxygen gradient when entering the OMZ region and with oxygen profiles of weaker than average vertical oxygen gradient when leaving the OMZ region (and depth-dependent consumption plus downward redistribution

BGD
9, 14291–14325, 2012

of oxygen happening inside the region). The western boundary circulation characterized by strong vertical shear is a likely candidate for generating sharp vertical oxygen gradients that could be transported within eastward current bands into the OMZ.

Appendix A

Dissipation rate parametrized from vessel mounted ADCP data

There is a widely known parametrization of dissipation rate ϵ for the open ocean (Polzin et al., 1995; Gregg et al., 2003), which is based on the concept of breaking internal waves causing turbulence, dissipation and mixing. Important needed parameters to use this parametrization are finescale vertical shear and finescale vertical strain; "finescale" in this context comprises vertical wavenumbers of order 10 to order 100 m. In this study, we had access to vertical shear via vmADCP data (Sect. 3.6), but for strain we lacked simultaneous data of satisfying quality. For remedy we fitted another parametrization with fewer parameters, using own data from the tropical North Atlantic Ocean, plus using data from midlatitudes, which were reported by Polzin et al. (1995) and formed the base of their parametrization.

Here two variables were used which have commonly been identified to influence mixing intensity in the open ocean: (1) the intensity of velocity vertical shear in the vertical wavelength band of tens to hundreds of meters, as providing the forcing, (2) the characteristic slope of internal waves, which influences their probability to break and cause turbulence, dissipation and mixing. The predictors Ψ_1 and Ψ_2 we defined for the parametrization were derived from these two variables, having been inspired by the Garrett-Munk (GM) internal wave model (Garrett and Munk, 1975; Munk, 1981). Ψ_1 was chosen proportional to the power spectral level Φ_S of vertical finescale shear as

$$\Psi_1 = N^2 \cdot G, \tag{A1}$$

BGD
9, 14291–14325, 2012

with N buoyancy frequency and G a nondimensional number describing the power spectral level of shear, Φ_S, in relation to its GM background level $\Phi_{S,GM} = \text{const.} \cdot N^2$. G was estimated from vmADCP data by

$$G = \frac{\Phi_S^{k_{min} \cdots k_{max}}}{\Phi_{S,GM}^{k_{min} \cdots k_{max}}}, \tag{A2}$$

and both $\Phi_S^{k_{min} \cdots k_{max}}$ and $\Phi_{S,GM}^{k_{min} \cdots k_{max}}$ were calculated in the vertical wavenumber range $k_{min} = 1/128$ cpm to $k_{max} = 1/38.4$ cpm by weighted averaging as $\Sigma((9-i)/8 \cdot \Phi_{S,i})/\Sigma((9-i)/8)$ for the appropriate $\Phi_{S,i}$ at wavenumbers $k_i = (2+i)/384$ cpm. This way to estimate G is specific to the used vmADCP configuration and the used depth interval for the analysis of 150 to 500 m. But G is not expected to be sensitive to the particular choice of k_i in the finescale range. Ψ_2 was chosen as

$$\Psi_2 = \frac{f}{N}, \tag{A3}$$

with f the Coriolis parameter, because the characteristic slope of the internal wave field approximately is a power of $f \cdot N^{-1}$ when assuming the GM model.

In order to fit a regression model we took the existing 45 stations with simultaneous microstructure profiles, CTD profile and vmADCP measurements, plus data from the High Resolution Profiler collected at several midlatitude locations as reported by Polzin et al. (1995). Predictor Ψ_1 relied on vmADCP data for G and CTD data for N^2, predictor Ψ_2 needed latitude and CTD data for N, and predictand ϵ was provided by microstructure data. In order to avoid a skewed distribution in parameter space we did linear regression in logarithmic space, i.e. the regression model was $\log \epsilon = a_0 + a_1 \cdot \log \Psi_1 + a_2 \cdot \log \Psi_2$. The best model fit (Fig. 8) can be written as

$$\epsilon = \frac{1}{100} \cdot \Psi_1^{4/3} \cdot \Psi_2^{5/9} \tag{A4}$$

BGD
9, 14291–14325, 2012

with multiple correlation $R^2 = 0.80$. This relation translates to

$$\epsilon = \frac{1}{100} \cdot f^{5/9} \cdot N^{19/9} \cdot G^{4/3}. \quad \text{(A5)}$$

Acknowledgements. This study benefitted from cruises, infrastructure and financial support by the German Federal Ministry of Education and Research through the co-operative projects SOPRAN and NORTH ATLANTIC, and by German Science Foundation's Sonderforschungsbereich SFB754 "Climate Biogeochemistry Interactions in the Tropical Ocean". We acknowledge the support of the European Commission (FP7-EuroSITES grant agreement No. 202955). The support of captains, crews and scientific crews of Meteor cruise 80, Meteor cruise 83/1, Merian cruise 08/1, Merian cruise 10/1, L'Atalante cruises GEOMAR/3 and GEOMAR/4 is highly appreciated. We thank Johannes Karstensen for fruitful discussions.

The service charges for this open access publication have been covered by a Research Centre of the Helmholtz Association.

References

Angel, M. V.: Vertical migrations in the oceanic realm: possible causes and probable effects, in: Migration: Mechanisms and Adaptive Significance, Contributions in Marine Science, suppl. Vol. 27, edited by: Rankin, M. A., Checkley, D., Cullen, J., Kitting, C., and Thomas, P., Marine Science Institute, Austin, Texas, 45–70, 1985. 14310

Banyte, D., Tanhua, T., Visbeck, M., Wallace, D. W. R., Karstensen, J., Krahmann, G., Schneider, A., Stramma, L., and Dengler, M.: Diapycnal diffusivity at the upper boundary of the tropical North Atlantic oxygen minimum zone, J. Geophys. Res., 117, C09016, doi:10.1029/2011JC007762, 2012. 14294, 14296, 14300, 14303, 14304

Bograd, S. J., Castro, C. G., Di Lorenzo, E., Palacios, D. M., Bailey, H., Gilly, W., and Chavez, F. P.: Oxygen declines and the shoaling of the hypoxic boundary in the California Current, Geophys. Res. Lett., 35, L12607, doi:10.1029/2008GL034185, 2008. 14293

BGD
9, 14291–14325, 2012

Bopp, L., Monfray, P., Aumont, O., Dufresne, J.-L., Le Treut, H., Madec, G., Terray, L., and Orr, J. C.: Potential impact of climate change on marine export production, Global Biogeochem. Cy., 15, 81–99, 2001. 14294

Bopp, L., Le Quere, C., Heimann, M., and Manning, A. C.: Climate-induced oceanic oxygen fluxes: Implications for the contemporary carbon budget, Global Biogeochem. Cy., 16, 1022, doi:10.1029/2001GB001445, 2002. 14294

Brandt, P., Hormann, V., Körtzinger, A., Visbeck, M., Krahmann, G., Stramma, L., Lumpkin, R., and Schmid, C.: Changes in the Ventilation of the Oxygen Minimum Zone of the Tropical North Atlantic, J. Phys. Oceanogr., 40, 1784–1801, doi:10.1175/2010JPO4301.1, 2010. 14294, 14295

Duteil, O. and Oschlies, A.: Sensitivity of simulated extent and future evolution of marine suboxia to mixing intensity, Geophys. Res. Lett., 38, L06607, doi:10.1029/2011GL046877, 2011. 14293, 14294

Ekau, W., Auel, H., Pörtner, H.-O., and Gilbert, D.: Impacts of hypoxia on the structure and processes in pelagic communities (zooplankton, macro-invertebrates and fish), Biogeosciences, 7, 1669–1699, doi:10.5194/bg-7-1669-2010, 2010. 14293

Feely, R. A., Sabine, C. L., Schlitzer, R., Bullister, J. L., Mecking, S., and Greeley, D.: Oxygen utilization and organic carbon remineralization in the upper water column of the Pacific Ocean, J. Oceanogr., 60, 45–52, 2004. 14310

Fischer, T.: Diapycnal diffusivity and transport of matter in the open ocean estimated from underway acoustic profiling and microstructure profiling, Ph.D. thesis, Leibniz Institute of Marine Sciences (GEOMAR), University of Kiel, Germany, 105 pp., 2011. 14302, 14305

Garcia, H. E., Locarnini, R. A., Boyer, T. P., Antonov, J. I., Baranova, O. K., Zweng, M. M., and Johnson, D. R.: World Ocean Atlas 2009 Volume 3 (Dissolved Oxygen, Apparent Oxygen Utilization, and Oxygen Saturation), NOAA Atlas NESDIS 70, edited by: Levitus, S., US Government Printing Office, Washington, DC, 344 pp., 2010. 14310, 14318, 14319

Gargett, A. E.: An investigation of the occurrence of oceanic turbulence with respect to finestructure, J. Phys. Oceanogr., 6, 139–156, 1976. 14301

Garrett, C. and Munk, W.: Space-time scales of internal waves: A progress report, J. Geophys. Res., 80, 291–297, 1975. 14311

Gregg, M. C.: Scaling turbulent dissipation in the thermocline, J. Geophys. Res., 94, 9686–9698, 1989. 14301

BGD
9, 14291–14325, 2012

Gregg, M., Sanford, T. B., and Winkel, D. P.: Reduced mixing from the breaking of internal waves in equatorial waters, Nature, 422, 513–515, 2003. 14305, 14311

Gruber, N.: Warming up, turning sour, losing breath: ocean biogeochemistry under global change, Philos. T. Roy. Soc. A, 369, 1980–1996, doi:10.1098/rsta.2011.0003, 2011. 14293, 14294

Helm, K. P., Bindoff, N. L., and Church, J. A.: Observed decreases in oxygen content of the global ocean, Geophys. Res. Lett., 38, L23602, doi:10.1029/2011GL049513, 2011. 14293

Ho, D. T., Ledwell, J. R., and Smethie Jr., W. M.: Use of SF_5CF_3 for ocean tracer release experiments, Geophys. Res. Lett., 35, L04602, doi:10.1029/2007GL032799, 2008. 14300

Karstensen, J., Stramma, L., and Visbeck, M.: Oxygen minimum zones in the eastern tropical Atlantic and Pacific oceans, Prog. Oceanogr., 77, 331–350, doi:10.1016/j.pocean.2007.05.009, 2008. 14292, 14295, 14308, 14310, 14324

Keeling, R. F., Körtzinger, A., and Gruber, N.: Ocean deoxygenation in a warming world, Annu. Rev. Mar. Sci., 2, 199–229, doi:10.1146/annurev.marine.010908.163855, 2010. 14293, 14294, 14308, 14310

Kunze, E., Firing, E., Hummon, J. M., Chereskin, T. K., and Thurnherr, A. M.: Global abyssal mixing inferred from lowered ADCP shear and CTD strain profiles, J. Phys. Oceanogr., 36, 1553–1576, 2006. 14301

Lam, P. and Kuypers, M. M. M.: Microbial nitrogen cycling processes in oxygen minimum zones, Annu. Rev. Mar. Sci., 3, 317–345, doi:10.1146/annurev-marine-120709-142814, 2011. 14293

Martin, J. H., Knauer, G. A., Karl, D. M., and Broenkow, W. W.: VERTEX: carbon cycling in the northeast Pacific, Deep-Sea Res., 34, 267–285, 1987. 14308

Matear, R. J. and Hirst, A. C.: Long-term changes in dissolved oxygen concentrations in the ocean caused by protracted global warming, Global Biogeochem. Cy., 17, 1125, doi:10.1029/2002GB001997, 2003. 14294

Meissner, K. J., Galbraith, E. D., and Völker, C.: Denitrification under glacial and interglacial conditions: A physical approach, Paleoceanography, 20, PA3001, doi:10.1029/2004PA001083, 2005. 14293

Munk, W. H.: Internal waves and small-scale processes, in: Evolution of Physical Oceanography; Scientific Surveys in Honor of Henry Stommel, edited by: Warren, B. A. and Wunsch, C., MIT press, Cambridge and London, 264–291, 1981. 14311

BGD

9, 14291–14325, 2012

Najjar, R. G., Jin, X., Louanchi, F., Aumont, O., Caldeira, K., Doney, S. C., Dutay, J.-C., Follows, M., Gruber, N., Joos, F., Lindsay, K., Maier-Reimer, E., Matear, R. J., Matsumoto, K., Monfray, P., Mouchet, A., Orr, J. C., Plattner, G.-K., Sarmiento, J. L., Schlitzer, R., Slater, R. D., Weirig, M.-F., Yamanaka, Y., and Yool, A.: Impact of circulation on export production, dissolved organic matter, and dissolved oxygen in the ocean: results from phase II of the Ocean Carbon-cycle Model Intercomparison Project (OCMIP-2), Global Biogeochem. Cy., 21, GB3007, doi:10.1029/2006GB002857, 2007. 14293

Oakey, N. S.: Determination of the rate of dissipation of turbulent energy from simultaneous temperature and velocity shear microstructure measurements, J. Phys. Oceanogr., 12, 256–271, 1982. 14300

Osborn, T. R.: Estimates of the local rat of vertical diffusion from dissipation measurements, J. Phys. Oceanogr., 10, 83–89, 1980. 14301

Oschlies, A., Schulz, K. G., Riebesell, U., and Schmittner, A.: Simulated 21st century's increase in oceanic suboxia by CO_2-enhanced biotic carbon export, Global Biogeochem. Cy., 22, GB4008, doi:10.1029/2007GB003147, 2008. 14294

Paulmier, A. and Ruiz-Pino, D.: Oxygen minimum zones (OMZs) in the modern ocean, Prog. Oceanogr., 80, 113–128, doi:10.1016/j.pocean.2008.08.001, 2009. 14292

Polzin, K. L., Toole, J. M., and Schmitt, R. W.: Finescale parameterizations of turbulent dissipation, J. Phys. Oceanogr., 25, 306–328, 1995. 14311, 14312, 14325

Polzin, K., Kunze, E., Hummon, J., and Firing, E.: The finescale response of lowered ADCP velocity profiles, J. Atmos. Ocean. Tech., 19, 205–224, 2002. 14301, 14302

Prince, E. D., Luo, J., Goodyear, C. P., Hoolihan, J. P., Snodgrass, D., Orbesen, E. S., Serafy, J. E., Ortiz, M., and Schirripa, M. J.: Ocean scale hypoxia-based habitat compression of atlantic istiophorid billfishes, Fish. Oceanogr., 19, 448–462, doi:10.1111/j.1365-2419.2010.00556.x, 2010. 14293

Shih, L. H., Koseff, J. R., Ivey, G. N., and Ferziger, J. H.: Parameterization of turbulent fluxes and scales using homogeneous sheared stably stratified turbulence simulations, J. Fluid Mech., 525, 193–214, 2005. 14301

Siedler, G., Zangenberg, N., and Onken, R.: Seasonal changes in the tropical Atlantic circulation: observation and simulation of the guinea dome, J. Geophys. Res., 97, 703–715, 1992. 14295

BGD
9, 14291–14325, 2012

Steinberg, D. K., Goldthwait, S. A., and Hansell, D. A.: Zooplankton vertical migration and the active transport of dissolved organic and inorganic nitrogen in the Sargasso Sea, Deep-Sea Res. Pt. I, 49, 1445–1461, 2002. 14310

Stips, A. and Prandke, H.: Recommended Algorithm for Dissipation Rate calculation within PROVESS, European Commission, JRC, Space Applications Institute, Technical Note No. 1.00.116, available at: www.pol.ac.uk/provess/bodc/doc/dissi_algo.pdf, last access: 10 October 2012, 2000. 14300

St. Laurent, L. and Schmitt, R. W.: The contribution of salt fingers to vertical mixing in the North Atlantic Tracer Release Experiment, J. Phys. Oceanogr., 29, 1404–1424, 1999. 14301, 14304, 14309

Stramma, L., Brandt, P., Schafstall, J., Schott, F., Fischer, J., and Körtzinger, A.: Oxygen minimum zone in the North Atlantic south and east of the Cape Verde islands, J. Geophys. Res., 113, C04014, doi:10.1029/2007JC004369, 2008a. 14295

Stramma, L., Johnson, G. C., Sprintall, J., and Mohrholz, V.: Expanding Oxygen-Minimum Zones in the Tropical Oceans, Science, 320, 655–658, doi:10.1126/science.1153847, 2008b. 14293, 14294

Stramma, L., Visbeck, M., Brandt, P., Tanhua, T., and Wallace, D. W. R.: Deoxygenation in the oxygen minimum zone of the eastern tropical North Atlantic, Geophys. Res. Lett., 36, L20607, doi:10.1029/2009GL039593, 2009. 14294

Stramma, L., Schmidtko, S., Levin, L. A., and Johnson, G. C.: Ocean oxygen minima expansions and their biological impacts, Deep-Sea Res. Pt. I, 57, 587–595, doi:10.1016/j.dsr.2010.01.005, 2010. 14293

Vaquer-Sunyer, R. and Duarte, C. M.: Thresholds of hypoxia for marine biodiversity, P. Natl. Acad. Sci. USA, 105, 15452–15457, doi:10.1073/pnas.0803833105, 2008. 14293

Whitney, F. A., Freeland, H. J., and Robert, M.: Persistently declining oxygen levels in the interior waters of the eastern subarctic Pacific, Prog. Oceanogr., 75, 179–199, doi:10.1016/j.pocean.2007.08.007, 2007. 14293

Wright, J. J., Konwar, K. M., and Hallam, S. J.: Microbial ecology of expanding oxygen minimum zones, Nat. Rev. Microbiol., Advance Online Publications, doi:10.1038/nrmicro2778, 2012. 14293

Wyrtki, K.: The oxygen minima in relation to ocean circulation, Deep-Sea Res., 9, 11–23, 1962. 14293

BGD
9, 14291–14325, 2012

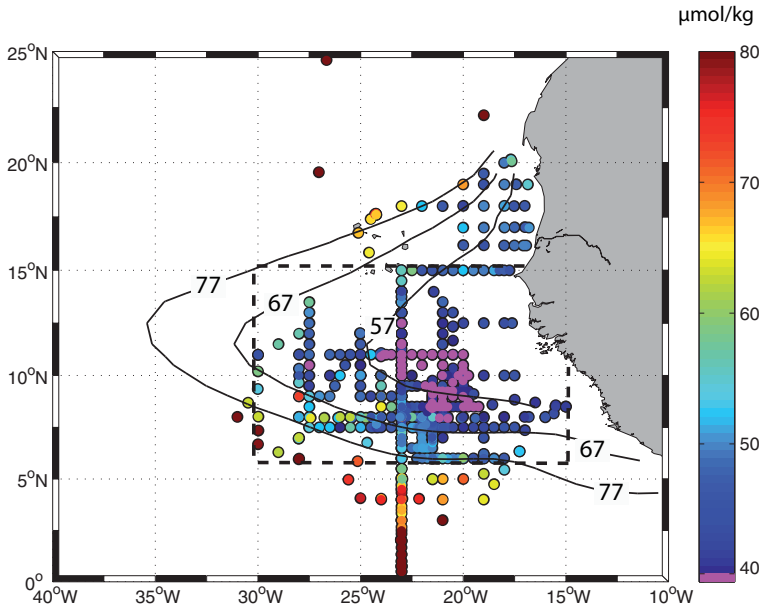

Fig. 1. Oxygen concentrations (coloured dots) in the core of the deep oxygen minimum, which is situated at depths between 350 and 500 m. Oxygen data was collected during the time period 2008 through 2010 of the simultaneous tracer release experiment GUTRE, and stems from 7 ship cruises in total. Black labelled lines are oxygen core concentration isolines, the minimum concentrations derived from World Ocean Atlas WOA09 (Garcia et al., 2010) by vertical spline interpolation. The WOA 77 µmol kg^{-1} and 67 µmol kg^{-1} isolines roughly encircle the observed 60 µmol kg^{-1} and 50 µmol kg^{-1} core concentrations in 2008 to 2010, while the WOA 57 µmol kg^{-1} isoline does not well describe the 40 µmol kg^{-1} observations. The WOA 77 / 60 µmol kg^{-1} observations line is used here to define the extent of the OMZ. The dashed black line defines the analysis box (in depth interval 150 to 500 m) that comprises most of the available mixing data.

BGD
9, 14291–14325, 2012

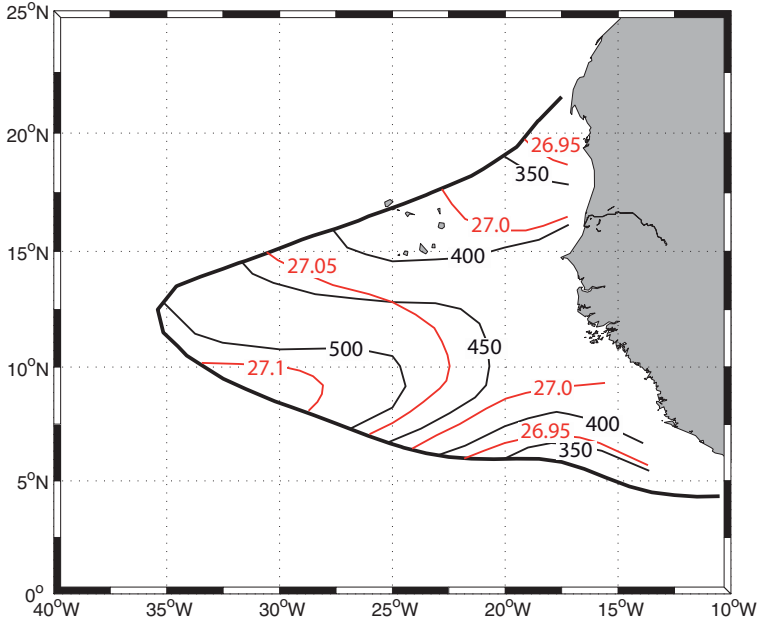

Fig. 2. Vertical position of the deep oxygen minimum core in depth coordinates (black isolines, meters) and in potential density coordinates (red isolines, kg m^{-3}). Isoline shapes are mostly derived from observations in 2008 to 2010. Where observational gaps were too large, isolines were completed by following the shapes of isolines based on World Ocean Atlas WOA09 (Garcia et al., 2010).

BGD
9, 14291–14325, 2012

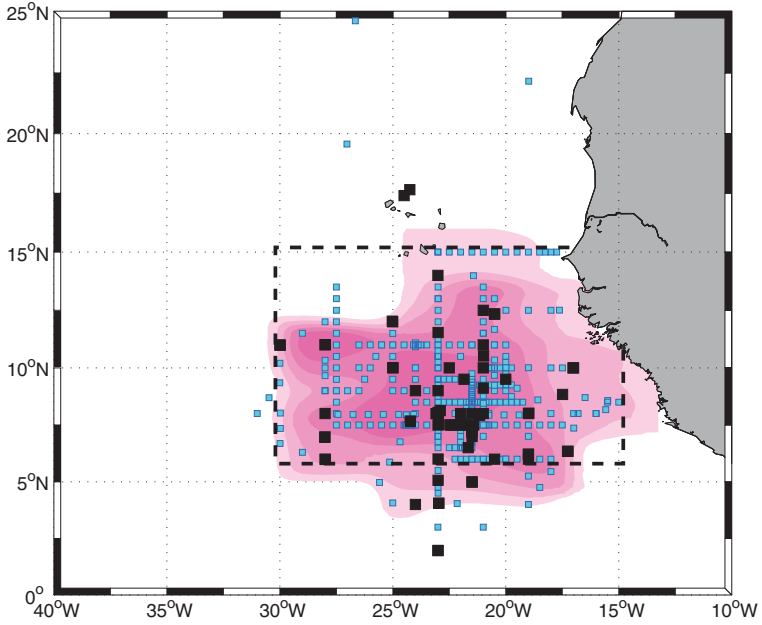

Fig. 3. Minimum covered area of tracer patch after 30 months (magenta filled contour) as well as locations of microstructure measurements (black squares) and stations with shear data from 75 kHz vessel mounted ADCP (blue squares) during cruises in 2008 to 2010. The chosen analysis box is marked with a dashed black line.

BGD
9, 14291–14325, 2012

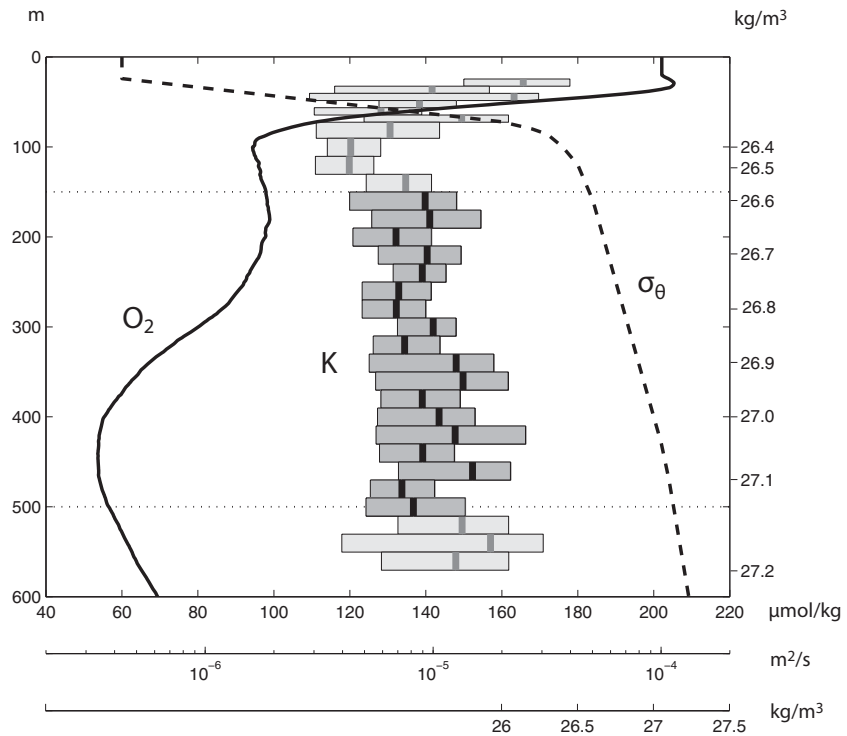

Fig. 4. Profiles of oxygen concentration, diapycnal diffusivity K from microstructure measurements, and potential density, averaged across the entire chosen analysis box in the OMZ. Dotted lines mark the depth interval where diapycnal oxygen flux will be evaluated. This is the depth interval where the depth ranges covered by the different methods to infer K overlap.

BGD
9, 14291–14325, 2012

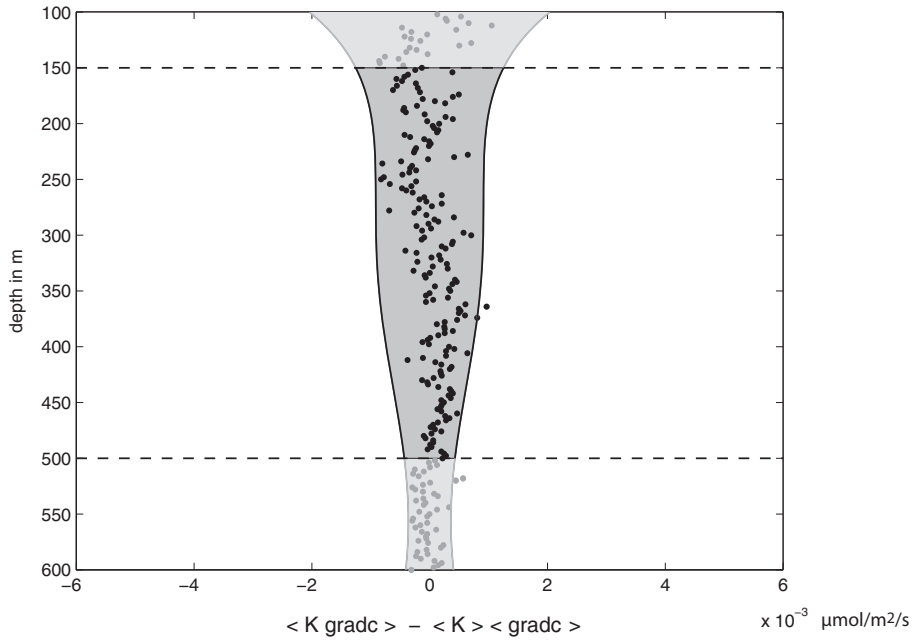

Fig. 5. Difference between the horizontal average of local diapycnal fluxes, and the product of horizontally averaged diapycnal diffusivity and horizontally averaged oxygen gradient, as a function of depth. The difference is found to be smaller than the 95 % confidence interval of $\langle K \cdot \mathrm{grad}\, c \rangle$ (grey shading) for most depth layers. Dashed lines mark the analysis depth interval. The evaluation outside the analysis depth interval assumes K values at each ship station to be constant through the 100 m to 600 m depth range.

BGD
9, 14291–14325, 2012

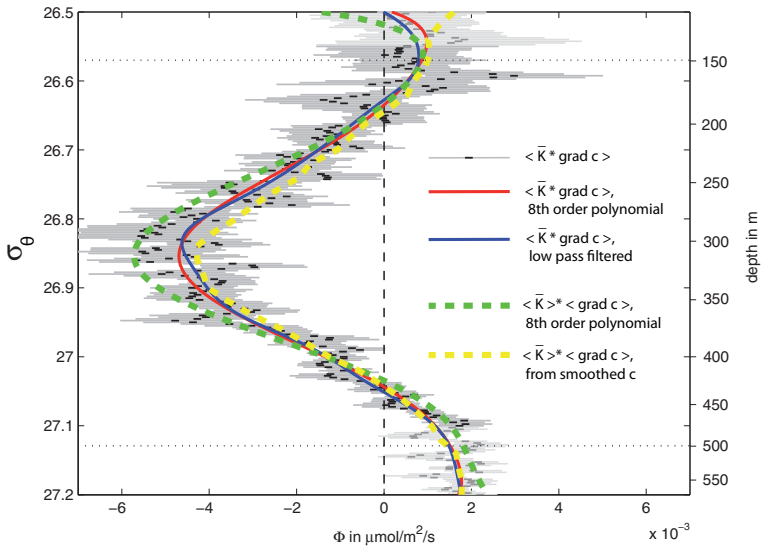

Fig. 6. Diapycnal oxygen flux in density coordinates as determined by different methods. The given smoothed curves assume that fluctuations of smaller vertical scales are an artefact of imperfect sampling. Black dots with grey shading: local oxygen gradients over 2 m combined with local K from MSS/ADCP measurements to local diapycnal flux, then averaged horizontally along isopycnals. Red line: Corresponding fitted 8th order polynomial. Blue line: corresponding low pass filtered flux profile. Dashed green line: 8th order polynomial on flux profile that was derived from horizontally averaged oxygen gradient and integral K value from the Tracer Release Experiment. Dashed yellow line: flux profile derived from vertically smoothed oxygen gradient profiles that have been horizontally averaged along isopycnals before combined with the integral K value from the Tracer Release Experiment. Dotted black lines approximately mark the analysis depth interval 150 to 500 m for which K estimates exist. The deep OMZ core is located at about σ_θ = 27.03 kg m^{-3} or 425 m. The deep oxycline is located at about σ_θ = 26.85 kg m^{-3} or 310 m.

BGD
9, 14291–14325, 2012

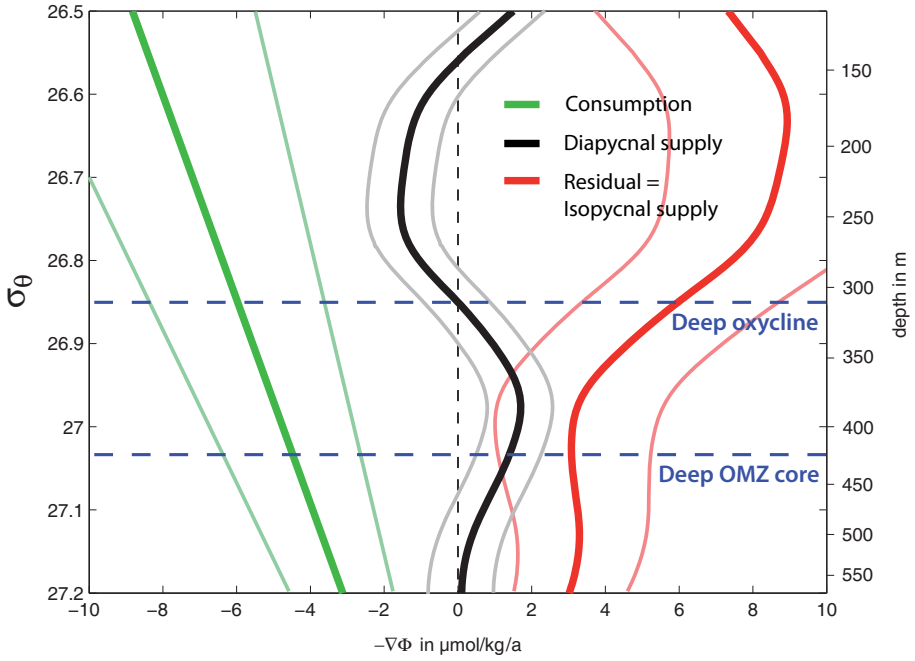

Fig. 7. Terms of the oxygen budget (diapycnal supply + isopycnal supply + consumption rate = 0) as a function of density. Diapycnal supply = negative diapycnal flux divergence (black) was determined in this study (here we chose a smooth line compromising between divergences of the polynomial and the low pass smoothed fluxes from TRE and MSS, as of Fig. 6). Oxygen consumption rate (green) was estimated according to Karstensen et al. (2008); the exponential decrease in depth coordinates turns out to be hardly discernible from linear when transformed to isopycnal coordinates in the depth interval 150 to 500 m. The residual that closes the budget must account for isopycnal supply (red). Uncertainties are 95 % confidence limits.

BGD
9, 14291–14325, 2012

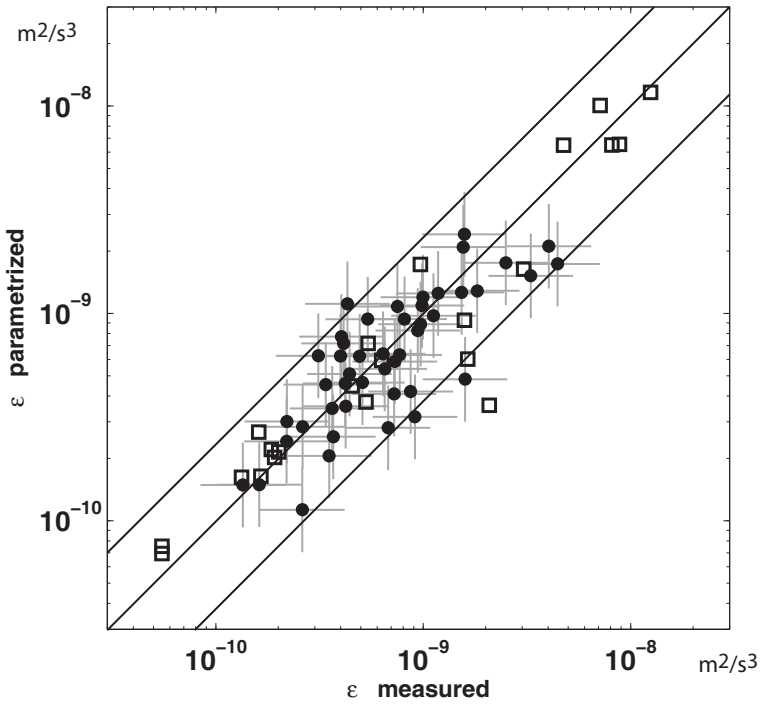

Fig. 8. Predicted versus measured turbulent dissipation rates. Predictions by parametrization $\epsilon = 1/100 \cdot f^{5/9} \cdot N^{19/9} \cdot G^{4/3}$ that resulted from a two-parameter-fit in $\Psi_1 = N^2 \cdot G$ (vertical shear power) and $\Psi_2 = f \cdot N^{-1}$ (internal wave slope). Measurements by microstructure profiler MSS90D in the region of the tropical North Atlantic OMZ (black dots) and values reported by Polzin et al. (1995) performed with the High Resolution Profiler in different midlatitude locations (squares). 95 % of predictions lie within a factor 2.5 from measured values.

BGD
9, 14291–14325, 2012